Talanta 89 (2012) 183–188

Contents lists available at SciVerse ScienceDirect

Talanta

journal homepage: www.elsevier.com/locate/talanta

Conduction mechanism and gas sensing properties of $CoFe_2O_4$ nanocomposite thick films for H_2S gas

Anjali B. Bodade[a], Archana B. Bodade[a], H.G. Wankhade[a], G.N. Chaudhari[a,*], D.C. Kothari[b]

[a] Nano Technology Research Laboratory, Department of Chemistry, Shri Shivaji Science College, Amravati 444602, MS, India
[b] Department of Physics, University of Mumbai, Vidyanagari, Santacruz (E), Mumbai 400 098, India

ARTICLE INFO

Article history:
Received 22 September 2011
Received in revised form 3 December 2011
Accepted 5 December 2011
Available online 8 December 2011

Keywords:
$CoFe_2O_4$
Ac conductivity
Sensitivity
Selectivity
H_2S Gas

ABSTRACT

Nanocrystalline 10 wt% Ni and 0.2 wt% Sm doped $CoFe_2O_4$ was prepared by sol–gel citrate method and calcined at different temperatures. The $CoFe_2O_4$ nanoparticles were characterized by X-ray diffraction (XRD), electrical properties were studied by impedance analysis. The XRD of $CoFe_2O_4$ shows cubic structure with grain growth of 40 nm. The ac conductivity was studied for the sample 10 wt% Ni and 0.2 wt% Sm doped $CoFe_2O_4$ calcined at 650 °C, at temperature range from 100 to 700 °C over a wide range of frequencies from 50 Hz to 200 kHz. The result indicates that the ac conductivity depend on temperature, frequency and concentration of dopant. Nanocrystalline 10 wt% Ni and 0.2 wt% Sm doped $CoFe_2O_4$ was found to be good H_2S sensor with high sensitivity and selectivity.

1. Introduction

Semiconductor metal-oxide based gas sensors are commonly used for environmental monitoring and industrial applications due to their advantages such as small dimensions, low cost and convenient operation [1,2]. The gas sensing mechanism of these sensors involves adsorption of atmospheric oxygen on the oxide surface that extracts electrons from the semiconducting material leading to change in carrier density and conductivity. On interaction with oxidizing or reducing gases, adsorbed oxygen concentration changes and thereby conductivity changes. The change in conductivity is a measure of gas concentration. For reducing gases such as H_2S and NH_3 the conductivity increases for n-type materials (as SnO_2 and ZnO) and reduces for p-type materials (as Te). The effect of oxidizing gases is opposite to that of reducing gases. Since the gas sensing mechanism is a surface reaction, use of nanostructured materials is expected to improve gas sensing characteristics.

Semiconducting metal oxides have been known for decades to be good gas sensing materials [3–12]. Ethanol sensors based on SnO_2 thick films have been commercialized for years. In 1991, Yamazoe [13] demonstrated that reduction in crystal size would significantly increase the sensor performance. This is because nanosized grains of metal oxides are almost depleted of carriers (most carriers are trapped in surface states) and exhibit much poorer conductivity than microsized grains in ambient air; hence, when exposed to target gases, they exhibit greater conductance changes as more carriers are activated from their trapped states to the conduction band than with microsized grains. Thus, the technological challenge moved to the fabrication of materials with nanocrystals which maintained their stability over long-term operation at high temperature [14]. The exploration of one-dimensional (1D) oxide nanostructures has been stimulated and facilitated by the convenience of obtaining large amounts of single crystalline nanowires/nanobelts via the vapor transport [15] and vapor–liquid–solid (VLS) methods [16].

The Sberveglieri [17] and Yang [18] groups initiated the investigation of gas sensing properties of SnO_2 nanobelts. Sberveglieri et al. [17] demonstrated the use of SnO_2 nanowires as sensor materials showing prominent current changes towards ethanol and CO, respectively, in a synthetic air environment, while Yang et al. [18] demonstrated the first photochemical NO_2 nanosensors (based on individual SnO_2 nanoribbons) operating at room temperature. In 2004, high performance ZnO nanowire sensors with a low detection limit of 1 ppm ethanol at 300 °C are reported [19]. Ever since then the number of reports on gas sensors based on 1D metal oxide nanostructures have been growing exponentially every year.

Even though the olfactory system of humans is exceptional at detecting and identifying many odours, most hazardous gases or vapours can only be recorded at too high concentrations or cannot be detected at all. Standardized methods for ambient air determination involve the use of various techniques and technologies as well as expensive and bulky equipment. All of the methods

* Corresponding author. Tel.: +91 721 2660255.
E-mail address: gnc4@indiatimes.com (G.N. Chaudhari).

0039-9140/$ – see front matter © 2011 Elsevier B.V. All rights reserved.
doi:10.1016/j.talanta.2011.12.013

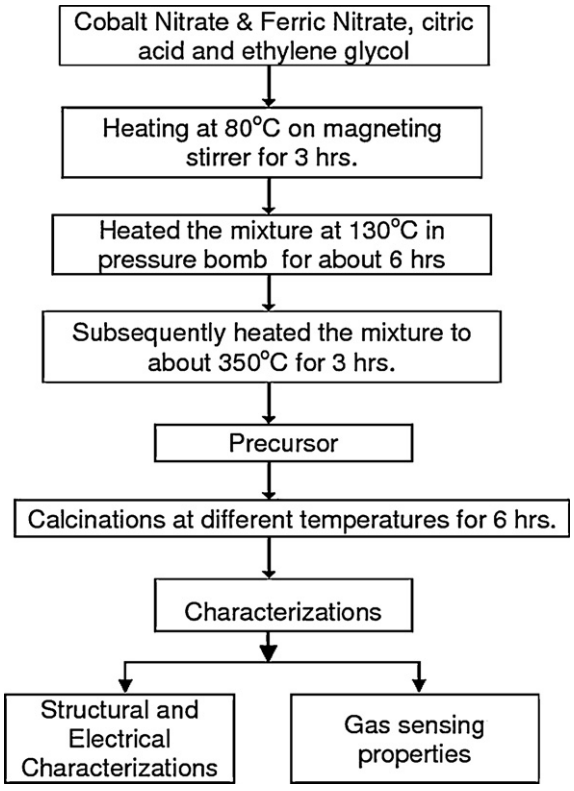

Fig. 1. Flow chart for the preparation of $CoFe_2O_4$ nanomaterials.

require laboratory procedures incapable of obtaining real-time results. However, serious attempts to control pollution demand that emissions of hazardous gases into the atmosphere be continuously monitored. Classical analytical methods are not suitable for such real-time analysis, and it follows that there is a need for developing rugged, reliable, small, and inexpensive equipment for air quality monitoring.

Monitoring of toxic H_2S gas is important in laboratories and industrial areas where it is being used as a process gas or generated as a byproduct. Also, H_2S is one of the most widely used bad-smelling gas which makes the surrounding environment unpleasant. Hence much attention has been paid to detect H_2S gas and develop H_2S sensing materials [20–23].

2. Experimental details

Nanocrystalline $CoFe_2O_4$ powder was synthesized by using sol–gel citrate method. Cobalt nitrate and ferric nitrate were used as raw materials. A stoichiometric mixture of nitrates was mixed with citric acid and ethylene glycol and stirred magnetically at 80 °C for 3 h to obtain a homogenous mixture; the solution was further heated in a pressure vessel at about 130 °C for 6 h and subsequently kept at 350 °C for 3 h. The dried powder was then calcined from 450 to 750 °C. In order to improve the crystallinity of the powder, sensitivity and selectivity of the material, nickel nitrate was added in the reaction mixture in the proper ratio. To improve the sensitivity it is further doped with the 0.2 wt% samarium. Synthesis of nanocrystalline $CoFe_2O_4$ is shown in the form of flow chart in Fig. 1.

3. Results and discussion

The X-ray pattern of the doped and undoped $CoFe_2O_4$ samples is depicted in Fig. 2. The positions and relative intensities of all the peaks indicate that the crystalline structure of the products favors the formation of cubic spinel phase only, which is accordant to JCPDS card NO. 22-1086. Moreover, the observed peak positions are consistent with the characteristic peaks reported for $CoFe_2O_4$ in the literature [24]. No other impurity phases are observed in 5 and 10 wt% Ni doped $CoFe_2O_4$ but one extra peak is observed in 15 wt% Ni doped $CoFe_2O_4$. Additionally, it clearly shows that the as-synthesized $CoFe_2O_4$ samples reveal broadening diffraction peak, which is due to the reduced particle size. The average grain size of

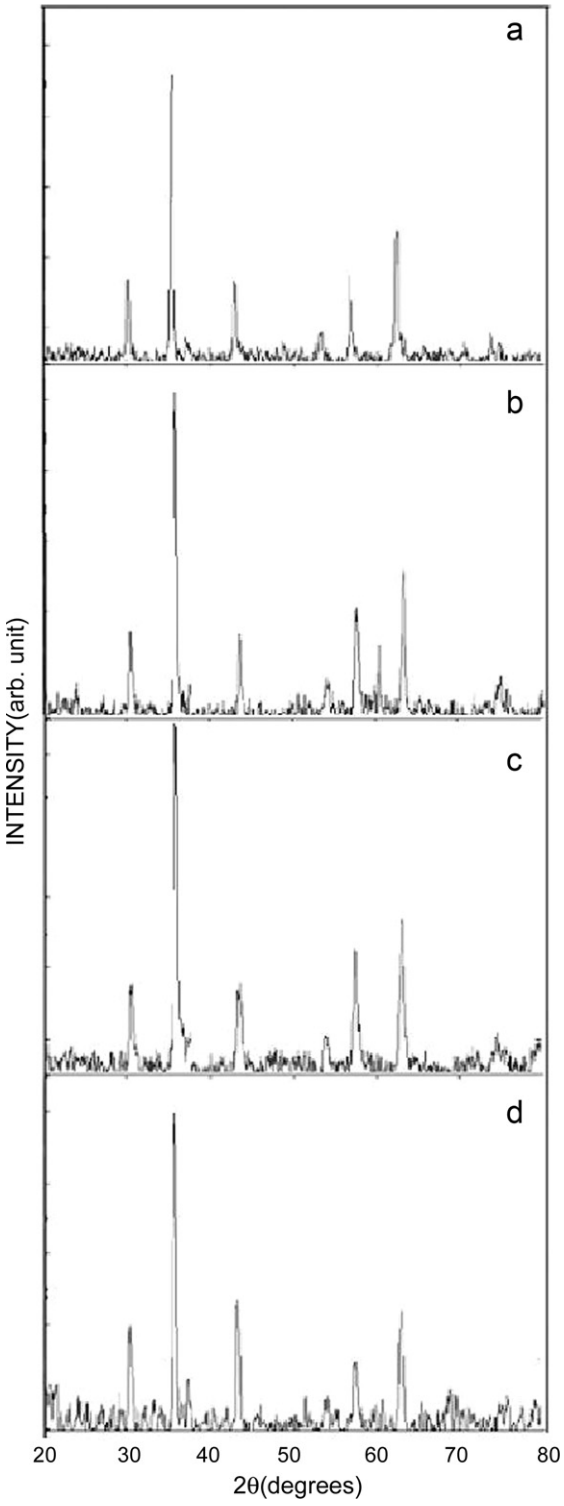

Fig. 2. X-ray diffraction of (a) $CoFe_2O_4$, (b) 5 wt% Ni doped $CoFe_2O_4$, (c) 10 wt% Ni doped $CoFe_2O_4$, and (d) 15 wt% Ni doped $CoFe_2O_4$.

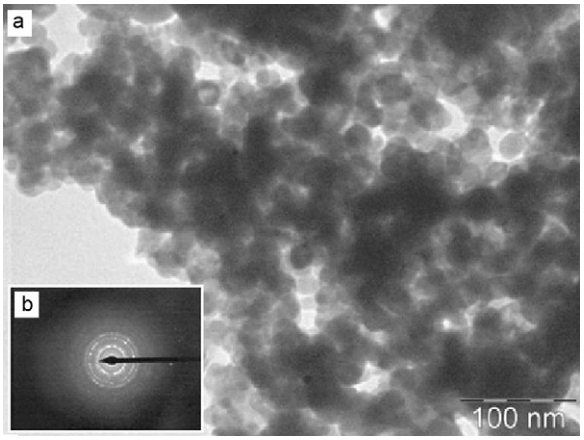

Fig. 3. TEM image of 0.2 wt% Sm and 10 wt% Ni doped $CoFe_2O_4$ calcined at 650 °C.

the as-synthesized nanoparticles calculated by Scherer's formula is 40 nm.

Fig. 3 shows TEM images of the $CoFe_2O_4$ nanoparticles obtained without any size-sorting process. It reveals that the as-synthesized nanoparticles were nearly monodisperse with spherical shape. The average particles size is 41 nm, which is in good agreement with the particle sizes estimated by Scherer's formula. This suggests that each individual particle is a single crystal [25]. The diffraction pattern shown for $CoFe_2O_4$ in Fig. 3b reveals the spotted ring like structure indicates the highly crystalline nature of the synthesized nanocrystalline 0.2 wt% Sm and 10 wt% Ni doped $CoFe_2O_4$ calcined at 650 °C.

In order to further elucidate the transport mechanism in nanocrystalline $CoFe_2O_4$ calcined at 650 °C sample, ac conductivity at different frequencies and temperatures, was determined by using the dielectric data as the following formula

$$\sigma(\omega) = \omega \cdot \varepsilon_0 \cdot \varepsilon''$$

where $\sigma(\omega)$ is the ac conductivity at a frequency ω ($\omega = 2\pi f$) and ε_0 is the permittivity of free space. The frequency dependence of the ac conductivity at different temperatures is shown in Fig. 4. At low frequencies, the conductivity shows a flat response which corresponds to the dc part of the conductivity. At higher frequencies, the conductivity shows dispersion. It is clear from the figure that the flat region increases with the increase in temperature. Fig. 4 shows an increase of the conductivity with increasing temperature indicating a characteristic activated behavior over the complete temperature range studied.

The activation energy for the nanocrystalline $CoFe_2O_4$, 10 wt% Ni doped $CoFe_2O_4$, 0.2 wt% Sm and 10 wt% Ni doped $CoFe_2O_4$ and for frequencies, varies from 10k to 200k were found to be (for $CoFe_2O_4$) 1.37877E-05, 1.81654E-05, 1.99061E-05, 1.55948E-04, 1.54156E-04, 1.51105E-04 eV (10 wt% Ni doped $CoFe_2O_4$) 1.53E-04, 1.3E-04, 1.19E-04, 1.17E-04, 1.15E-04 eV, and (0.2 wt% Sm and 10 wt% Ni doped $CoFe_2O_4$) 1.02253E-04, 1.00866E-04, 1.00039E-04, 9.97716E-05, 9.81429E-05, 9.45667E-05 eV, respectively. From Fig. 5 it is to be noted that the value of activation energy is less for nanocrystalline 0.2 wt% Sm and 10 wt% Ni doped $CoFe_2O_4$ and decreases with increasing frequency in a regular fashion as compared to $CoFe_2O_4$, 10 wt% Ni doped $CoFe_2O_4$.

The impedance data for nanocrystalline $CoFe_2O_4$ calcined at 650 °C have been measured in the temperature range from 100 to 700 °C. Fig. 6 shows the Nyquist plot of the impedance measurements. The decrease of resistance with increasing temperature is a well-known property of semiconducting materials. All measurements on this particle size exhibit an almost semicircle indicating that the single conduction mechanism is involved in the

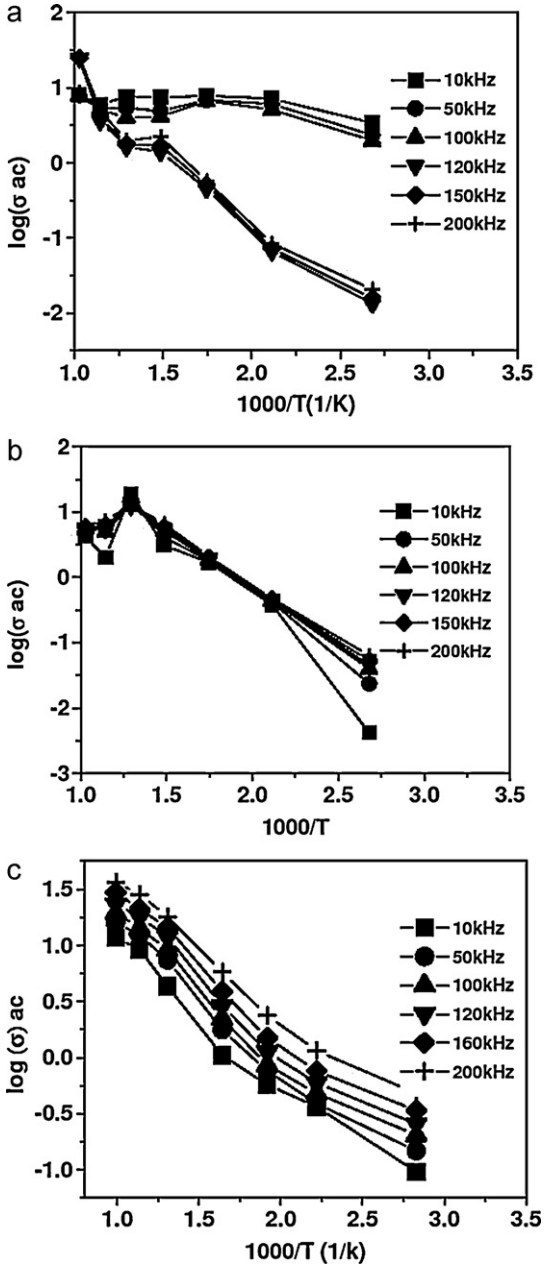

Fig. 4. Arrehenius plot for temperature dependent conductivity for (a) $CoFe_2O_4$ (b) 10 wt% Ni doped $CoFe_2O_4$, (c) 0.2 wt% Sm and 10 wt% Ni doped $CoFe_2O_4$.

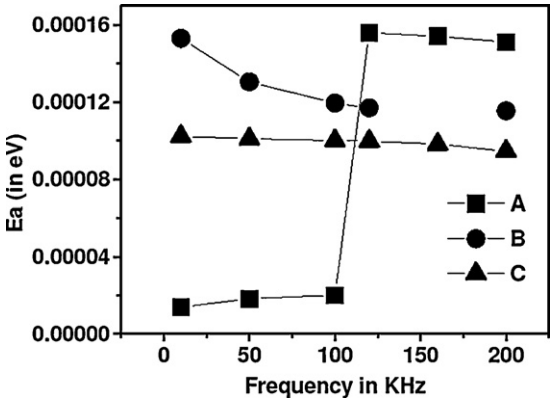

Fig. 5. Variation of activation energy with frequency for nanocrystalline (A) $CoFe_2O_4$, (B) 10 wt% Ni doped $CoFe_2O_4$, (C) 0.2 wt% Sm and 10 wt% Ni doped $CoFe_2O_4$.

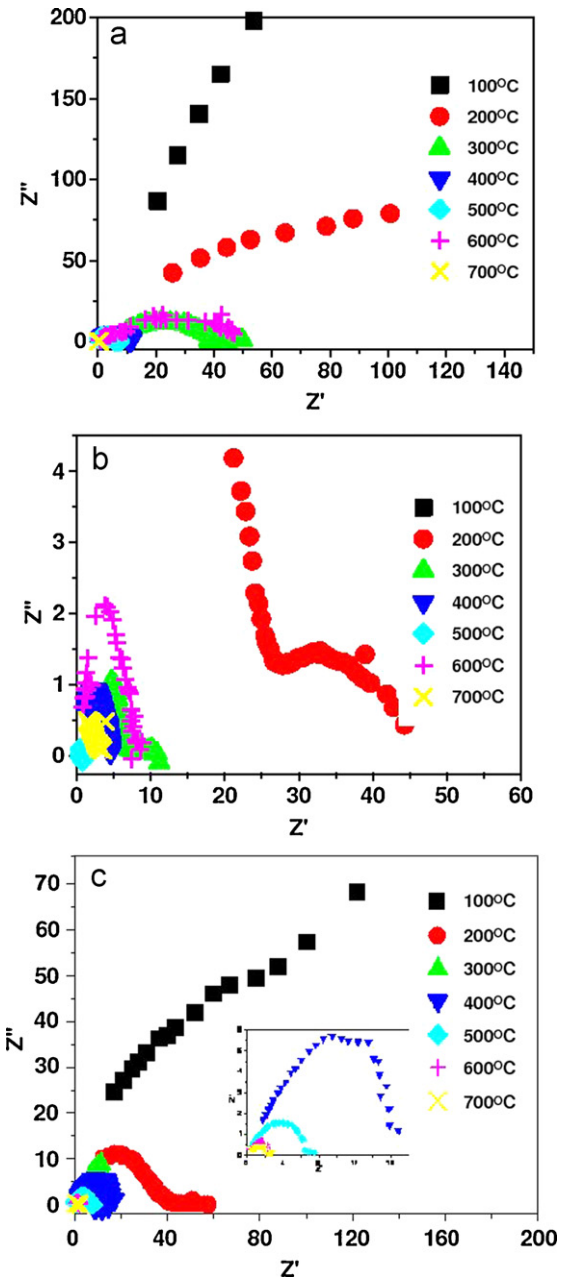

Fig. 6. Nyquist plot for (a) $CoFe_2O_4$, (b) 10 wt% Ni doped $CoFe_2O_4$, (c) 0.2 wt% Sm and 10 wt% Ni doped $CoFe_2O_4$.

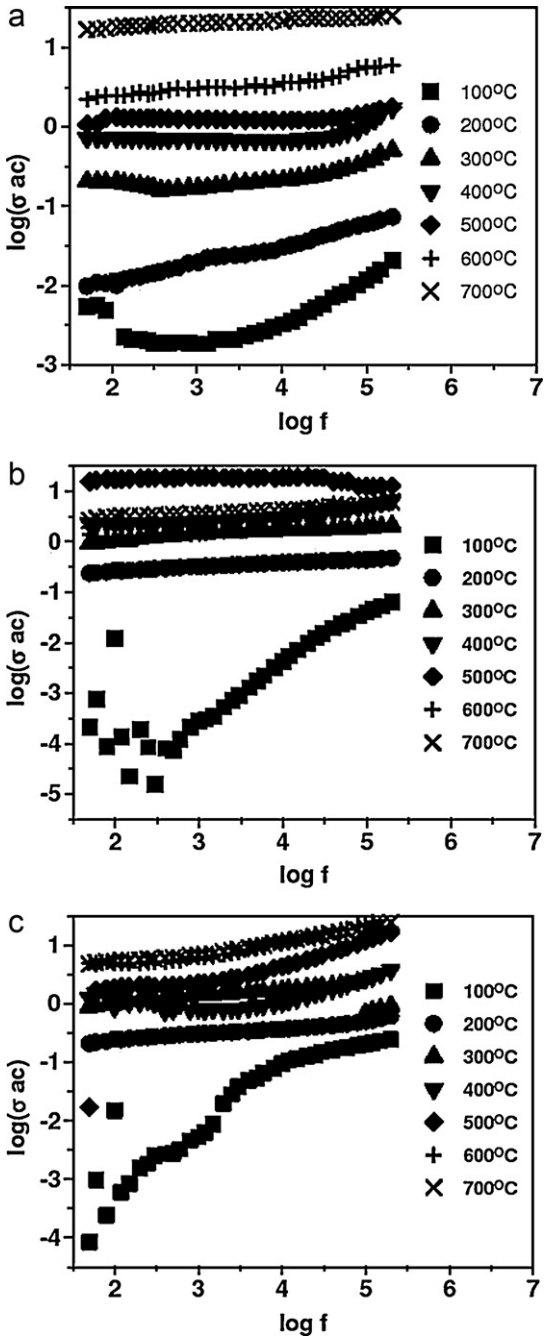

Fig. 7. Variation of ac conductivity with frequency for (a) $CoFe_2O_4$, (b) 10 wt% Ni doped $CoFe_2O_4$, and (c) 0.2 wt% Sm and 10 wt% Ni doped $CoFe_2O_4$.

composite system. This single conduction mechanism may be attributed to grain site or may be due to the mobility of free charges induced by increase in temperature. The semicircle obtained decreases gradually with the increase of temperature showing that the sample is more conductive at higher temperature.

In Nyquist plots, these semi circle arcs represent different relaxation processes. Usually semi circle at lower frequency represents grain boundary relaxation process and the one at higher frequencies gives the information on grain relaxation. It is evident from Nyquist plots that grains are contributing to the physical properties of the polycrystalline sample.

The ac conductivity increases with increase of the frequency and temperature applied in the experiment. The increase in conductivity on increasing the frequency and temperature is a common response for semiconductor material. It is due to the tremendous increase of the mobility of charge carriers in the composite film. As shown in Fig. 7, there are two trends appeared, the first one is frequency independent conductivity and another is frequency dependent conductivity. The first trend is contributed by free charges available in the composite system whereas the second, which is frequency dependent conductivity, is due to trapped charges which are only active at higher frequency region. From Fig. 7, it is clear that 0.2 wt% Sm and 10 wt% Ni doped $CoFe_2O_4$ calcined at 650 °C shows better conductivity even at lower temperature as compared to the 10 wt% Ni doped $CoFe_2O_4$ and undoped $CoFe_2O_4$.

Fig. 8 shows the effect of calcination temperatures on the response of $CoFe_2O_4$ sensors to 1000 ppm H_2S gas in an operating temperatures of 50–350 °C. Although the maximum responses of $CoFe_2O_4$ obtained at different heating temperatures appear at

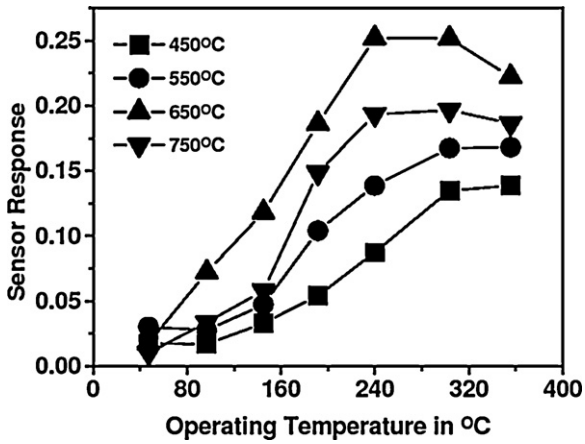

Fig. 8. Sensor response to 1000 ppm H_2S as a function of the operating temperature for undoped $CoFe_2O_4$ films calcined at 450, 550, 650 and 750 °C.

different operating temperatures, it is clearly seen that the responses to H_2S gas are greatly affected by the heating temperature. The response of $CoFe_2O_4$ obtained at 650 °C for 6 h reached a maximum at an operating temperature of 250 °C.

In order to promote gas sensitivity, dopants were shown to effectively influence the semiconductive properties of sensor materials. Fig. 9 shows the different wt% (5, 10 and 15) of Ni doped $CoFe_2O_4$ calcined at 650 °C for 6 h for 1000 ppm H_2S gas of an

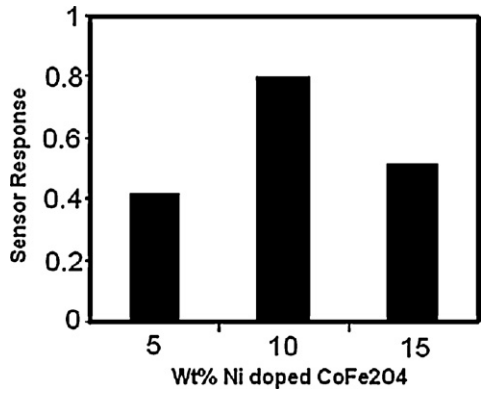

Fig. 9. Sensor response of 5%, 10% and 15% Ni-doped $CoFe_2O_4$ films calcined at 450, 550, 650 and 750 °C for 1000 ppm H_2S gas at an operating temperature 200 °C.

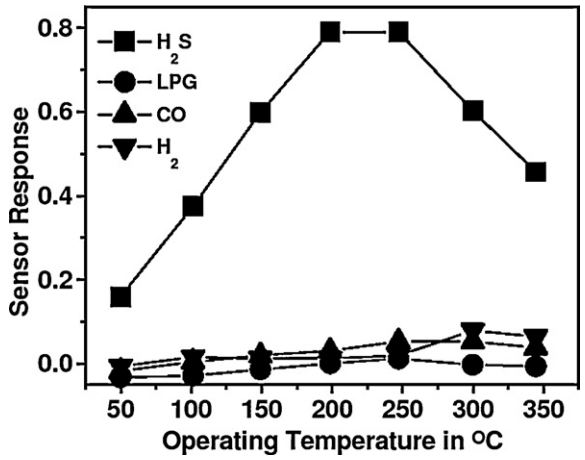

Fig. 10. Sensor response of 0.2 wt% Sm and 10 wt% Ni doped $CoFe_2O_4$ thick films calcined at 650 °C to 1000 ppm of H_2S, LPG, CO and H_2 as a function of operating temperature.

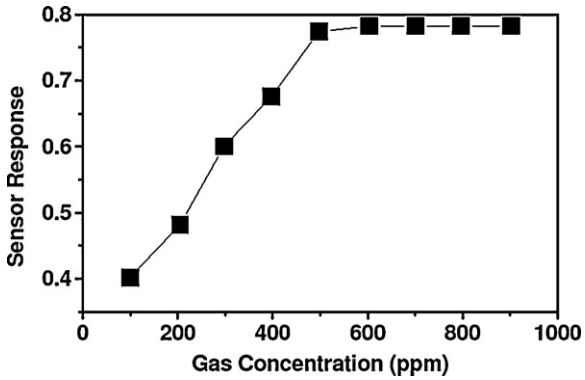

Fig. 11. Sensor response at 200 °C to H_2S as a function of the gas concentration of 0.2 wt% Sm and 10 wt% Ni doped $CoFe_2O_4$ thick films calcined at 650 °C.

operating temperature 250 °C. The gas response of the $CoFe_2O_4$ was markedly promoted for 10 wt% Ni doped $CoFe_2O_4$ calcined at 650 °C. Furthermore the 10 wt% Ni doped $CoFe_2O_4$ nanocomposite material was modified by doping with different wt% of Sm. The sensitivity is found to be further increased with 0.2 wt% of Sm in 10 wt% Ni doped $CoFe_2O_4$.

Selectivity is the ability that a gas sensor to distinguishes between different kinds of gases. Fig. 10 shows the cross sensitivity of 0.2 wt% of Sm and 10 wt% Ni doped $CoFe_2O_4$ for H_2S, CO, LPG and NH_3 gases as a function of operating temperature. It is evident from the figure that towards 0.2 wt% of Sm and 10 wt% Ni doped $CoFe_2O_4$ sensor was highly selective for H_2S as compare to CO, LPG and NH_3 gases. The sensor shows high degree of selectivity towards H_2S gas than other reducing gases.

As a function of H_2S concentration in air at the operating temperature of 200 °C, the response characteristics of the gas sensor were measured at different H_2S concentration from 100 ppm to 1000 ppm and the correlation curve between the concentration of H_2S and the response of the gas sensor is shown in Fig. 11. With increasing H_2S gas concentration, the response increases rapidly from 100 ppm and reaches saturation beyond 500 ppm.

Generally, the decrease of electrical resistance of a semiconductor sensor element upon contact with a reducing gas originates from a consumption of adsorbed or surface oxygen of the oxide used. Thus, the H_2S sensitivity is small when the H_2S oxidation activity is small ($CdIn_2O_4$). When the activity is too large (15 wt% Ni doped $CdIn_2O_4$), the sensitivity for H_2S gas is again suppressed, because H_2S molecules are then consumed at the surface region of the sensor element, being unable to penetrate into the inner region. Only when the catalytic activity is at a suitable level in between 0.2 wt% Sm and 10 wt% Ni doped $CdIn_2O_4$, H_2S can diffuse into the inner region of the sensor element and

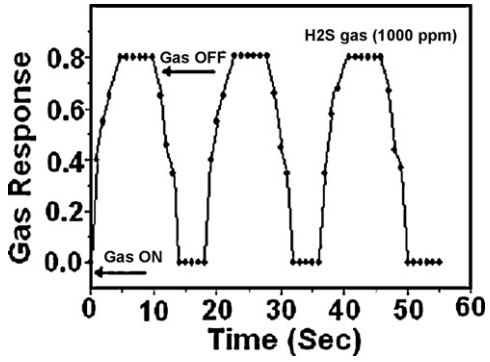

Fig. 12. Response characteristics of 0.2 wt% Sm in 10 wt% Ni doped $CoFe_2O_4$ calcined at 650 °C.

react with the adsorbed oxygen there, giving rise to a large sensitivity value. Thus, it is considered that the doubly promoted element has the most suitable activity at 200 °C among the various systems tested.

The response and recovery time of the most sensitive 0.2 wt% Sm in 10 wt% Ni doped $CoFe_2O_4$ calcined at 650 °C is represented in Fig. 11. The response was quick (5 s) and the recovery time was 20 s, at 200 °C to H_2S gas for 1000 ppm gas concentration (Fig. 12).

4. Conclusion

$CoFe_2O_4$ doped with various percents of Ni and Sm has been studied as a promising sensitive material for H_2S gas sensor. The sharp and single diffraction peaks of XRD confirm the formation of polycrystalline $CoFe_2O_4$ nanomaterials. The electrical conductivity of $CoFe_2O_4$ is strongly dependent on the amount of Ni doped $CoFe_2O_4$. The electrical conductivity increased with increasing Ni content and attained the maximum at 10 wt% Ni doped $CoFe_2O_4$ calcined at 650 °C. The impedance spectra for 10 wt% Ni doped $CoFe_2O_4$ shows the sample resistance decreases with increase in temperature. The sensor shows high degree of selectivity towards H_2S gas than other reducing gases. The best sensor response was found at an operating temperature of 200 °C for H_2S gas.

Acknowledgements

This work was financially supported by the University Grants Commission (UGC), New Delhi, India, under Major Research Project [Project no. F. No. 38-210/2009 (SR)].

References

[1] A. Khanna, R. Kumar, S.S. Bhatti, Appl. Phys. Lett. 82 (2003) 4388.
[2] T. Yamazaki, S. Wada, T. Noma, T. Suzuki, Sens. Actuators B14 (1993) 594.
[3] G.F. Fine, CavanaghF L.M., A. Afonja, R. Binions, Sensors 10 (2010) 5469–5502.
[4] C. Wang, L. Yin, L. Zhang, D. Xiang, R. Gao, Sensors 10 (2010) 2088–2106.
[5] K.J. Choi, H.W. Jang, Sensors 10 (2010) 4083–4099.
[6] J. Huang, Q. Wan, Sensors 9 (2009) 9903–9924.
[7] N. Tamaekong, C. Liewhiran, A. Wisitsoraat, S. Phanichphant, Sensors 9 (2009) 6652–6669.
[8] T. Zhai, X. Fang, M. Liao, X. Xu, H. Zeng, B. Yoshio, D. Golberg, Sensors 9 (2009) 6504–6529.
[9] S.M. Kanan, O.M. El-Kadri, I.A. Abu-Yousef, M.C. Kanan, Sensors 9 (2009) 8158–8196.
[10] A.P. Caricato, A. Luches, R. Rella, Sensors 9 (2009) 2682–2696.
[11] A.M. Paoletti, G. Pennesi, G. Rossi, A. Generosi, B. Paci, V.R. Albertini, Sensors 9 (2009) 5277–5297.
[12] R. Moos, K. Sahner, M. Fleischer, U. Guth, N. Barsan, U. Weimar, Sensors 9 (2009) 4323–4365.
[13] N. Yamazoe, Sens. Actuators B 5 (1991) 7–19.
[14] E. Comini, C. Baratto, G. Faglia, M. Ferroni, A. Vomiero, G. Sberveglieri, Prog. Mater. Sci. 54 (2009) 1–67.
[15] Z.W. Pan, Z.R. Dai, Z.L. Wang, Science 291 (2001) 1947–1949.
[16] A. Morales, C.A. Lieber, Science 279 (1998) 208–211.
[17] E. Comini, G. Faglia, G. Sberveglieri, Appl. Phys. Lett. 81 (2002) 1869–1871.
[18] M. Law, H. Kind, B. Messer, F. Kim, P.D. Yang, Angew. Chem. Int. Ed. 41 (2002) 2405–2408.
[19] Q. Wan, Q.H. Li, Y.J. Chen, T.H. Wang, X.L. He, J.P. Li, C.L. Lin, Appl. Phys. Lett. 84 (2004) 3654–3657.
[20] S. Yamauchi, Chemcial Sensor Technology, vol. 4, Kodansha, Tokyo, 1992.
[21] V.R. Katti, A.K. Debnath, K.P. Muthe, M. Kaur, A.K. Dua, S.C. Gadkari, S.K. Gupta, V.C. Sahni, Sens. Actuators B 96 (2003) 245–252.
[22] J. Tamaki, K. Shimanoe, Y. Yamada, Y. Yamamoto, N. Miura, N. Yamazoe, Sens. Actuators B 49 (1998) 121–125.
[23] W. Yuanda, T. Maosong, H. Xiuli, Z. Yushu, D. Guorui, Sens. Actuators B 79 (2001) 187–191.
[24] C.D. Culiță, G. Marinescu, L. Patron, N. Stănică, Revue Roumaine de Chimie 51 (2006) 503–508.
[25] S.H. Sun, H. Zeng, D.B. Robinson, S. Raoux, P.M. Rice, S.X. Wang, G.X. Li, J. Am. Chem. Soc. 126 (2004) 273.